Geophysical Journal International

Geophys. J. Int. (2018) **214,** 2084–2097
Advance Access publication 2018 June 19
GJI Seismology

doi: 10.1093/gji/ggy237

Secondary microseisms of North Atlantic windstorms in Central Eurasia—an understanding of an anomalously big bulge of seismic noise before the 2001 November 14 M_w 7.8 Kunlun earthquake

X. G. Hu

State Key Laboratory of Geodesy and Earth's Dynamics, Institute of Geodesy and Geophysics, Chinese Academy of Sciences. E-mail: hxg432@whigg.ac.cn

Accepted 2018 June 18. Received 2018 June 13; in original form 2017 November 16

SUMMARY

Three days before the M_w 7.8 earthquake on 2001 November 14 at Kunlun, China, an anomalously big bulge of seismic noise was observed at stations in Central Eurasia. The big bulge event has attracted considerable attention as it seem to be generated near the epicentre, and it has been suggested to indicate the occurrence of a possible slow-earthquake event related to the large earthquake. Investigating observations at seismic stations widely distributed in Eurasia, I show that the big bulges are most likely strong secondary microseisms caused by an extreme windstorm in the North Atlantic. By wide-angle triangulation of the measured azimuths of the bulge signals at 15 stations, I show the presence of a source region along the west coast of Norway and the north coast of Scotland/Great Britain. Using a wavelet-packet analysis method, I show that the secondary microseisms from North Atlantic windstorm can travel very far in Eurasia, reaching the Pacific coast of China, but they are strong attenuated on their way to North America. Without the obstruction of the Tibetan Plateau, secondary microseisms caused by severe European windstorms often form apparent bulges at stations in Central Eurasia. I further show, considering seismic noise spectra recorded over 20 years by stations distributed from Central Eurasia to East Asia, that North Atlantic windstorms play much more important roles than West Pacific and North Indian Ocean windstorms in generating seismic noise in Central Eurasia, causing significant seasonal variations of the seismic noise levels. Seismic noise variations recorded in Central Eurasia may therefore be used to study the long-term effects of Arctic and North Atlantic windstorms on local climate change.

Key words: Asia; Atlantic Ocean; Europe; Pacific Ocean; Seismic noise; Wave propagation.

1 INTRODUCTION

This study starts from observing an anomalously big bulge of seismic noise at Chinese Xinjiang seismic network on 2001 November 11, 3 d before the 2001 Novermber 14 M_w 7.8 earthquake at Kunlun, China. The strong earthquake occurred along the Kusai Lake-Kunlun pass fault of the Kunlun fault system (Fu & He 2005), and it was the most powerful quake in China for 5 decades (Li & Chen 2002). Fig. 1 show the big bulge signals observed at WMQ and WUS. The two seismic stations are located in Central Eurasia and near the epicentre of the large earthquake, for example, WMQ located about 800 km away from the epicentre. The source of the bulge signals seems to be near the epicentre because the peak of the bulge signals is almost as large as the peak of the signal from a local earthquake of M_w 3.5 (Yong *et al.* 2003). In the absence of earthquakes, oceanic secondary microseisms are the strongest signals recorded by continental seismic stations, and super oceanic storms can cause big bulge signals in seismic noise recorded by continental stations (Longuet-Higgins 1950). However, seismic station in Central Eurasia, such as WMQ, is one of the furthest stations from oceans on Earth. The West Pacific Ocean is the nearest ocean to Central Eurasia. Previous study indicated that strong West Pacific typhoons near the coasts of China cannot generate big bulges in secondary microseismic signals recorded at WMQ (Hu & Hao 2009). Thus, the cause for the bulge event before the 2001 Kunlun earthquake has attracted attention of Chinese scientists, and some of them inferred the big bulges as signals of a possible pre-sliding of the KunLun fault before the large earthquake (e.g. Yong *et al.* 2003; Mei *et al.* 2009; Wang *et al.* 2014).

No study has ruled out the possibility that North Atlantic windstorms may lead to the big bulge event, mainly because seismic stations in Central Eurasia are much farther away from the North Atlantic coast than from the West Pacific coast. People may take it for grant that secondary microseisms caused by North Atlantic windstorms in Central Eurasia are much weaker than those by West Pacific typhoons. In this study I investigate 6-d seismic noise signals before the 2001 Kunlun earthquake at the scale of Eurasia,

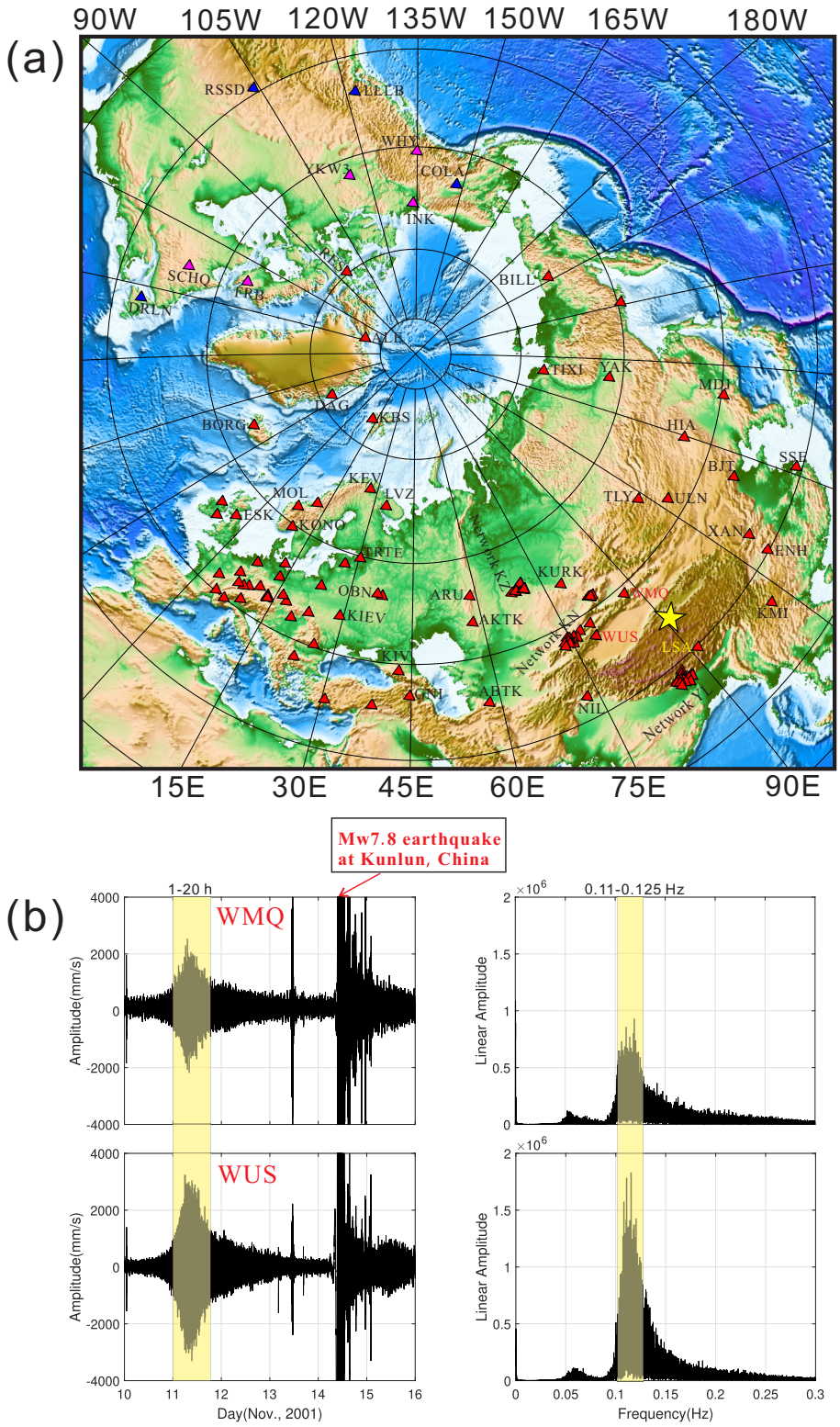

Figure 1. (a) Map showing seismic stations in Eurasia and North America used in this study. The yellow star indicates the epicentre of the M_w 7.8 earthquake at Kunlun, China on 2001 November 14. (b) Big bulges in seismic noise recorded at WMQ and WUS on 2001 November 11, 3 d before the M_w 7.8 KunLun earthquake. The two stations are located approximately 800 and 1000 km from the epicentre. Amplitude spectra for 20-hr bulge signals at the two stations show that the main components of the signals are concentrated in the narrow frequency band of 0.1–0.125 Hz. Many other stations in Eurasia, which are marked as red triangles on the map, also recorded big bulges in seismic noise on 2001 November 11.

showing that the big bulge signals at stations in Central Eurasia are strong secondary microseisms originated from the Norwegian Sea. Consulting previous studies (e.g. Reistad *et al.* 2011; Feng *et al.* 2012) on North Atlantic severe windstorms in the Norwegian

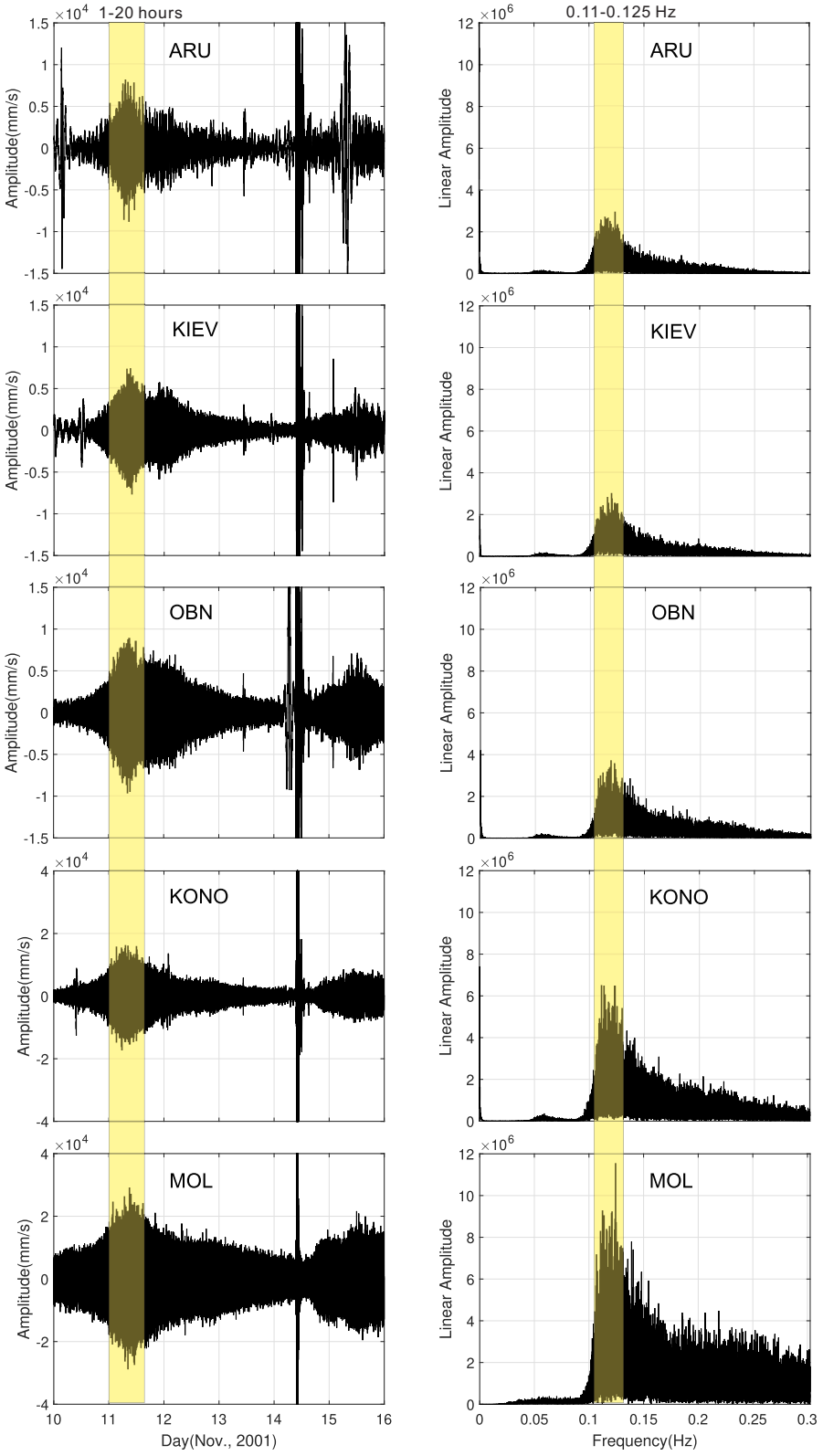

Figure 2. Significant bulge signals in seismic noise recorded at station ARU, OBN, KIEV, KONO and MOL on 2001 November 11. Data used here are vertical components of seismographs (LHZ). Seismic spectra for the 20-hr bulge signals during 11 November at the five stations show that the main components of the bulge signals are concentrated in the frequency band of 0.1–0.125 Hz. The closer the stations are to the Norwegian coast, the bigger bulges they record.

Sea, I verify that an unnamed North Atlantic extreme cyclone was very active in the Norwegian Sea on 2001 November 11. The big bulge signals in fact are strong secondary microseisms caused by the unnamed windstorm. In order to locate the source region of

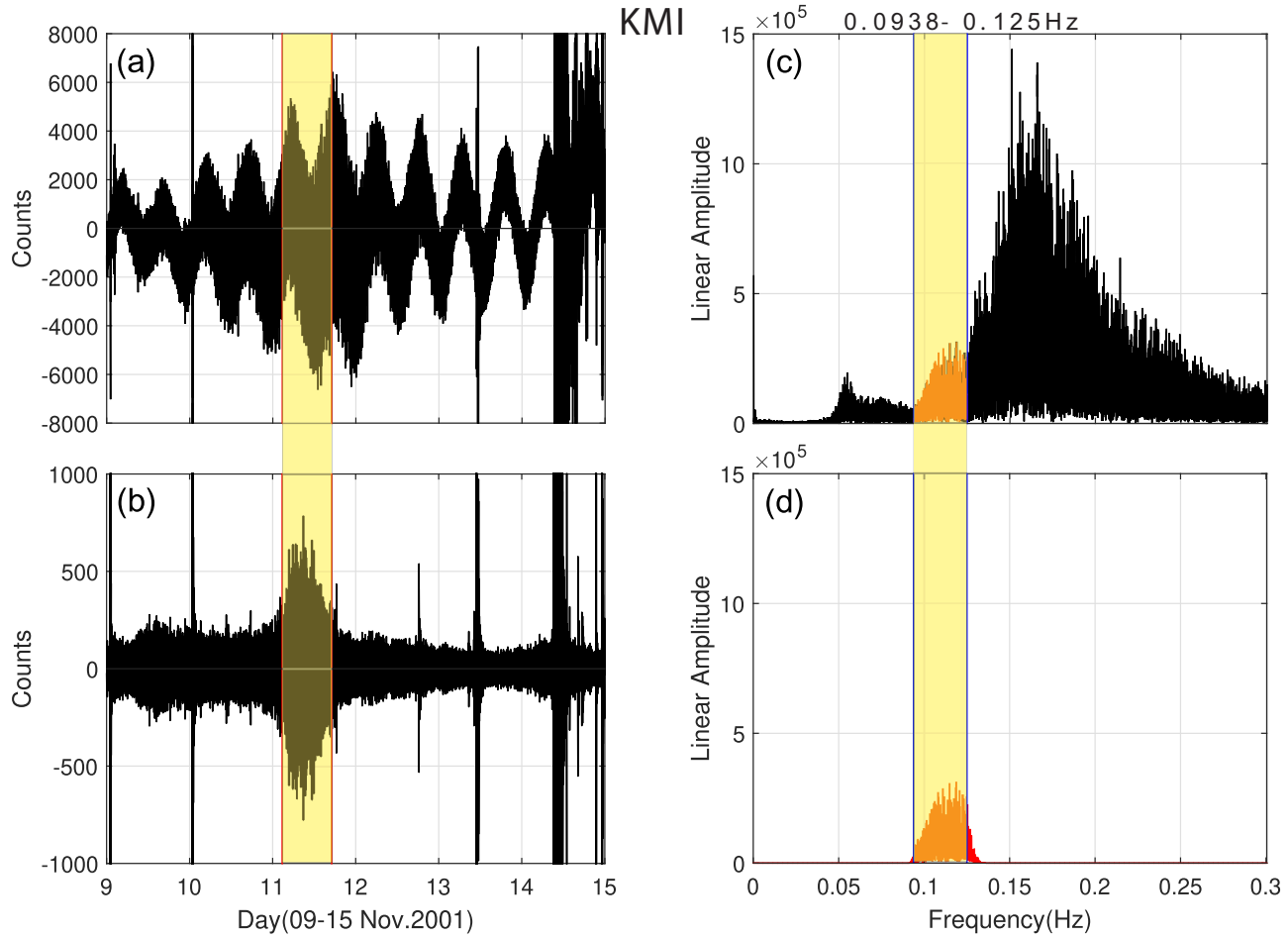

Figure 3. An Example showing the advantage of the wavelet-packet filter in extracting weak signals in a narrow frequency band. Figure (a) and (b) show raw vertical data(LHZ) and filtered data (in 0.0938–0.125 Hz) at station KMI, and a yellow color bar covers bulge signals (18 hr data) in the filtered data, indicating that the bulge signals caused by the North Atlantic windstorm on 2001 November 11 cannot be identified in the raw data but are apparent in the filtered data. Panels (c) and (d) show amplitude spectrum for 18-hr raw data and 18-hr filtered data, respectively, and a yellow colour bar highlights spectra in 0.0938–0.125 Hz, indicating that wavelet-packet filter exactly extracts data in 0.0938–0.125 Hz after clearly removing the main components of raw data in 0.13–0.2 Hz, which are secondary microseisms caused by the typhoon LingLing (Hu *et al.* 2009).

the big bulge in Central Eurasia, I compute the polarization of the bulge signals at a number of Eurasia stations. I also show that devastating North Atlantic extratropical cyclones, so-called European windstorms (Martínez-Alvarado *et al.* 2012; Hewson & Neu 2015), often generates apparent big bulge signals in seismic noise recorded in Central Eurasia.

To better understand secondary microseisms in Central Eurasia caused by North Atlantic windstorms, I further study of spectra of seismic noise over the years 1996–2016 for stations distributed from Central Eurasia to East Asia. I show that North Atlantic windstorms can generate much stronger seismic noise in Central Eurasia than West Pacific typhoons and North Indian Ocean cyclones do because of the influence of Tibetan Plateau structure on the propagation of Rayleigh waves. North Atlantic windstorms plays leading role in generating obvious seasonal fluctuation of seismic noise levels in Central Eurasia.

2 DATA AND METHODOLOGY

Oceanic secondary microseisms are the main component of seismic noise in recording of continental seismic stations. Oceanic waves generate microseisms by coupling atmospheric energy into the crust mainly in the form of Rayleigh waves, which occupy two peaks in the period band of 5–25 s (frequencies in 0.04–0.2 Hz) on seismic noise spectra, and body waves and Love waves are also observed in microseimsic noise fields (e.g. Friedrich *et al.* 1998). The primary microseisms (periods in 10–25 s) are generated by ocean gravity waves near coast (Hasselmann 1963). The secondary microseisms (periods in 5–12 s) are generated by standing ocean waves formed by non-linear interaction of propagating waves of similar periods traveling in opposite directions (Longuet-Higgins 1950). Sources of secondary microseimic noise in the form of second order pressure fluctuations due to opposing wave interactions are located at the sea surface and are not attenuated with depth (Longuet Higgins 1950). Strong secondary microseisms caused by powerful oceanic storms, such as cyclones or typhoons, can form significant bulges in seismic noise recorded by continental stations.

To study if secondary microseisms of North Atlantic windstorms are responsible for the big bulge recorded at seismic stations near the epicentre of the Kunlun earthquake, I have considered seismic noise recorded at stations widely distributed in Eurasia, North American region near Arctic and Greenland (Fig. 1). Data of those stations

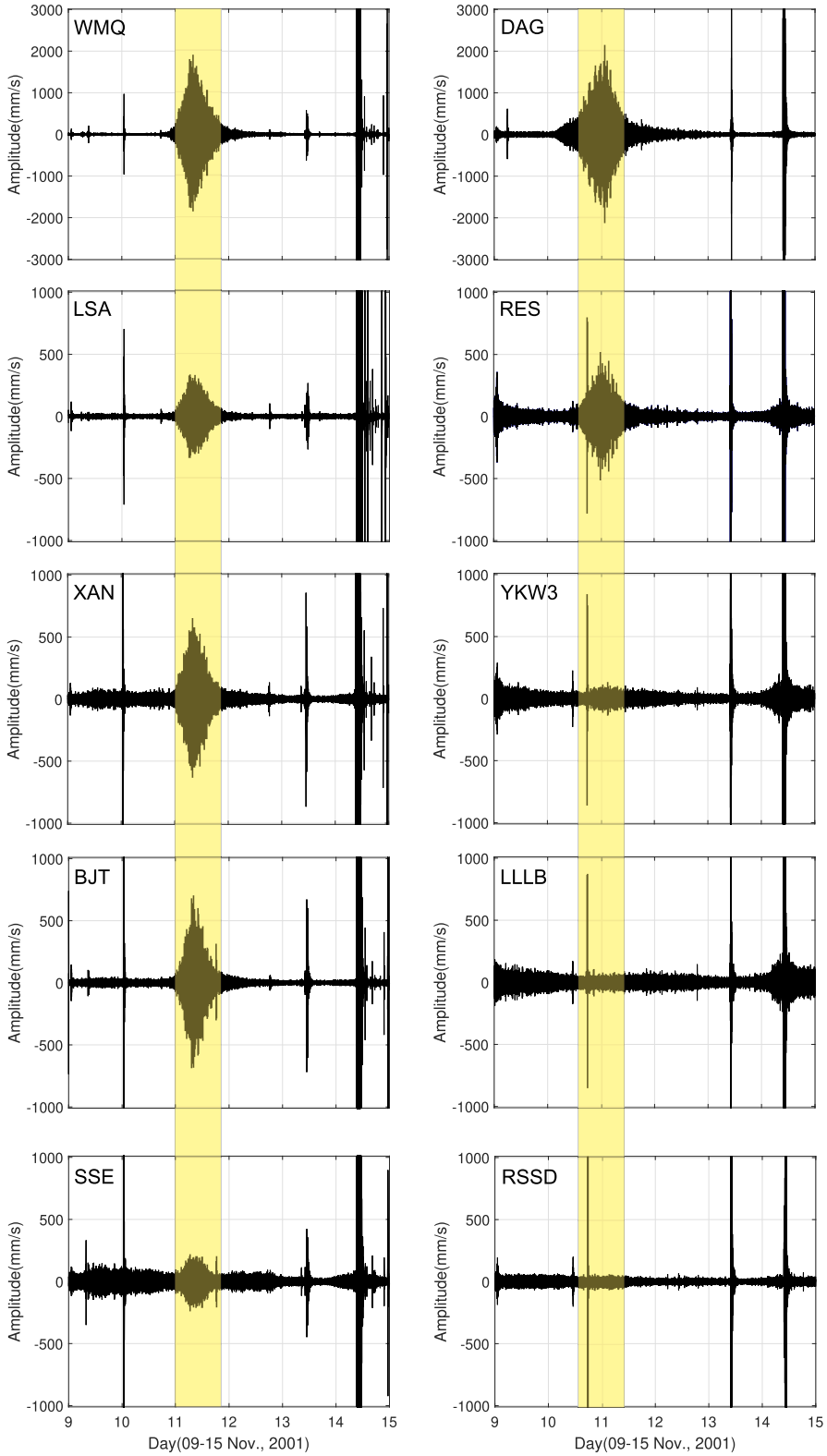

Figure 4. Filtered vertical data in the frequency band of 0.0938–0.125 Hz at 10 seismic stations. The bulge signals caused by the North Atlantic cyclone on 11 November (highlighted by a yellow bar) is apparent at Chinese station SSE, which is located about 9000 km away from the Norwegian Sea, but no similar bulge signals are visible at Canadian stations LLLB and RSSD.

were retrieved from the Incorporated Research Institutions for Seismology (IRIS) Data Management System. To observe bulge signals, I have processed 6 d of 1 sample s^{-1} continuous velocity time-series

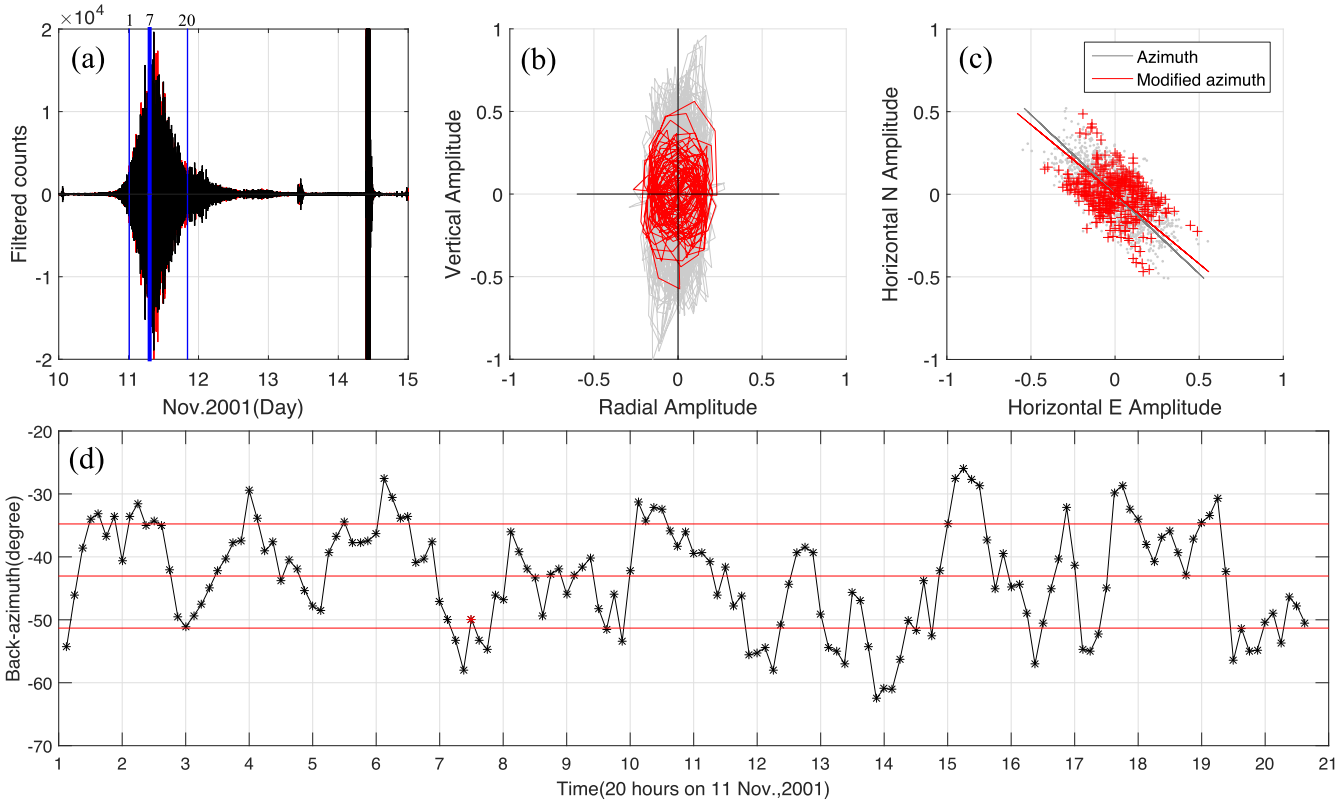

Figure 5. An example showing how to estimate the backazimuth range of the bulge signals for station KIEV on 2001 November 11. (a) Filtered horizontal data (time-series of displacement) in 0.0938–0.125 Hz. The red curve is the LHE data and black one the LHN data. The 20-hr bulge signals between the two blue lines (marked 1 and 20) is parsed into 157 overlapping segments (1800 s per segment) and then used to estimate backazimuths of source region for the bulge signals. The thick blue line marked seven indicates the 7th hr after the 20-hr bulge signals onset. (b) and (c) Hodogram showing the particle motion within the 52nd segment in the 7th hr. The red track in (b) is formed by 358 points corresponding to instantaneous motion ellipses with the ratio of the semiminor axis to the semimajor axis >3. The grey line in (c) is the initially estimated azimuth and the red one is the modified azimuth after the polarization analysis of instantaneous motion ellipse. (d) Backazimuth variation of the microseismic sources for KIEV. The black star points are backazimuths derived from the 157 overlapping segments in the 20-hr data, in which a red point is from the 52nd segment in the 7th hr. The three red lines are the average of backazimuths and standard deviations of the average, respectively.

(from 2001 November 9 to 14). Calibrated seismic records at periods greater than 2 s were obtained by deconvolving the instrument responses from the raw spectra. I have performed Fourier analysis to compare frequency characteristics of bulge signals at different stations. The bulge data were windowed using prolate tapers before computing Fourier transforms. A number of stations in Eurasia record the similar bulge signals on 11 November and their main components are concentrated in a very narrow frequency band of 0.1–0.125 Hz (Fig. 2).

In order to compare bulge signals in time-frequency domain among Eurasia stations and locate the source region of the bulge signals, I tried to extract the bulge signals in a narrow frequency band. I have found that standard bandpass filters, such as FIR filters, cannot work well for exactly extracting weak signals in a narrow frequency band. I filter the bulge data by using orthogonal wavelet filter formed by discrete wavelet-packet transform (DWPT) (Wickerhauser 1994). Orthogonal wavelet filter built by long Daubechies wavelet (Daubechies 1992) is suitable for exactly extracting low frequency signals in a narrow frequency band, as it is a zero-phase as well as causal filter without Gibbs phenomenon, and it has readily adjustable centre frequency and perfectly symmetrical passbands (e.g. Hu *et al.* 2006a,b, 2007). In this study, Daubechies wavelet with 1022 coefficients is used as the mother wavelet for DWPT, which form an orthogonal bandpass filter having frequency response close to 'brick-wall' (Hu *et al.* 2006a,b). As the bulge signals are in 0.1–0.125 Hz and the observation data have sample rate of 1 sample s^{-1}, decomposition level is set as 4 and analysis node as (4, 2) in DWPT. In such a setting, the bulge data can be filtered into the narrow frequency band $3/2^5$–$4/2^5$ Hz (i.e. 0.0938–0.125 Hz).

Determining the locations of seismic noise sources and their variation with time and frequency is a challenge. Secondary microseisms are predominantly fundamental mode Rayleigh waves, and the backazimuths between source region and stations can be determined by using signal processing techniques such as beamforming or polarization analyses (e.g. Cessaro 1994; Friedrich *et al.* 1998; Chevrot *et al.* 2007; Gerstoft & Tanimoto 2007; Brooks *et al.* 2009; Koper *et al.* 2010; Schimmel *et al.* 2011a; Behr *et al.* 2013). Beamforming extracts the correlated portions of the microseisms from a dense seismic network to determine their backazimuths, whereas polarization analyses enable the determination of backazimuths for individual station. The exact source location of conversion of ocean waves into seismic waves is often difficult to determine by back projecting source azimuths, due to the complexity of the secondary microseism excitation and no distance information in backazimuth data. However, wide-angle triangulation of the measured secondary microseism azimuths can be used to constrain source region (e.g. Cessaro 1994; Schimmel *et al.* 2011b). Elliptical retrograde polarization of secondary microseisms (Rayleigh waves) can be recorded

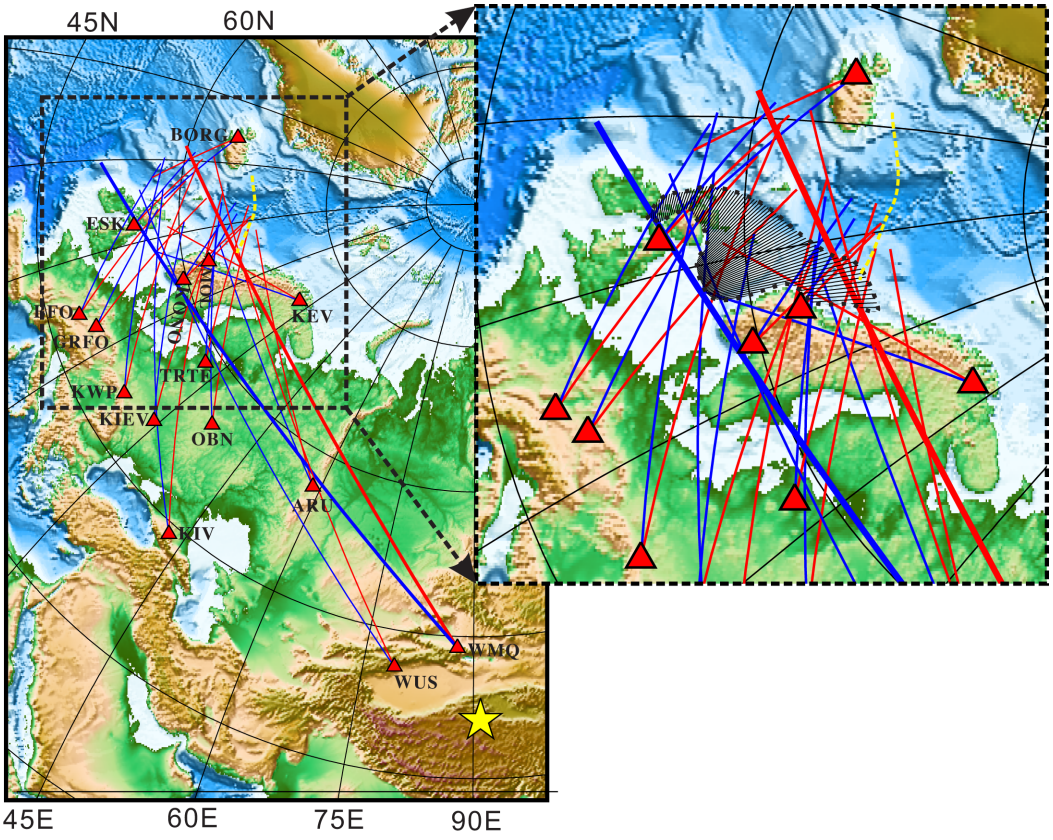

Figure 6. Geographical map showing a source region defined by backazimuth ranges for 15 stations. The red triangles represent the locations of the stations, and the red and blue lines from each triangle indicate backazimuth range for the bulge signals at the station. In the magnified view, the area covered by thin black lines represents the most possible source region that produce the big bulge signals in Central Eurasia. The thick yellow dot line indicates the trajectory of the super cyclone in North Atlantic on 2001 November 11 [Magnar Reistad *et al.* 2011].

by stations located on rocky ground (e.g. Tanimoto & Riveira 2005; Tanimoto *et al.* 2006), and it is the case for most Eurasia seismic stations. The analysis of the time-frequency representation of the three components of the seismogram enables us to determine semi-major and semi-minor axes of the ellipse retrograde polarization that best fits the ground motion, which indicating backazimuths of secondary microseism sources for a certain station (e.g. Schimmel & Gallart 2003, 2004). For big bulge of secondary microseisms caused by super cyclone, back projecting source azimuths for a number of stations may define a range including the sources of secondary microseisms.

I try to define a source region that produce the big bulge signals according to back projection of backazimuths between the source region and a number of stations that are widely distributed in the North Europe and Central Eurasia. Azimuth determination is based on polarization analysis of the Rayleigh waves during the bulge event. In my polarization analysis in the time-frequency domain, seismic noise data are firstly filtered into the frequency band of 0.0938–0.125 Hz by using the wavelet-packet filter, and then bulge data at a certain station is parsed into 1800 s segments, overlapping with each other by 75 per cent. According to the polarization attribute of Rayleigh waves in the horizontal plane, the propagation azimuth of the Rayleigh waves (radial direction) for the station is estimated initially from the horizontal component data according to the formula AZI = arctan (A_E/A_N), where A_E and A_N is mean absolute amplitudes for horizontal East and North component, respectively. To correct for the bias in the estimation, instantaneous polarization attributes of Rayleigh waves in the vertical plane, such as semi-major and semi-minor axes of the elliptic motion, are characterized by using complex trace analysis method (e.g. René *et al.* 1986; Galiana-Merino *et al.* 2011). The data points that have instantaneous elliptical motions with a ratio of semi-minor axis to semi-major axis greater than 3 are used for calculation backazimuth. Averaging corrected backazimuths for all segments and computing standard deviation of the average, we can obtain a range of azimuthal variation during the bulge event at the station.

To understand the influence of North Atlantic windstorms on seismic noise level in Central Eurasia, I have considered amplitude variations of power spectral density (PSD) for seismic noise data over the years 1996 and 2016 at stations distributed from Central Eurasia to West Pacific coast of Eurasia. An iterative process is performed to eliminate earthquake signals prior to the PSD estimation. In order to eliminate signals of large earthquakes without damaging large bulge microseismic signals, the process is first performed on the data of a day to remove data with amplitudes 8–10 times larger than the average amplitude of the day, and then the process is performed on the data of an hour in the day to remove data with amplitudes three times larger than the average amplitude of the hour , so as to remove signals of small earthquakes. Data are windowed by using Hamming tapers before estimation PSD of each hour. Averaging the PSD spectral amplitude over an hour enables the determination of a sequence of hourly PSD, and averaging hourly PSD over 24 hr enables the determination of a sequence of daily PSD. To display seasonal variations of seismic noise levels, a

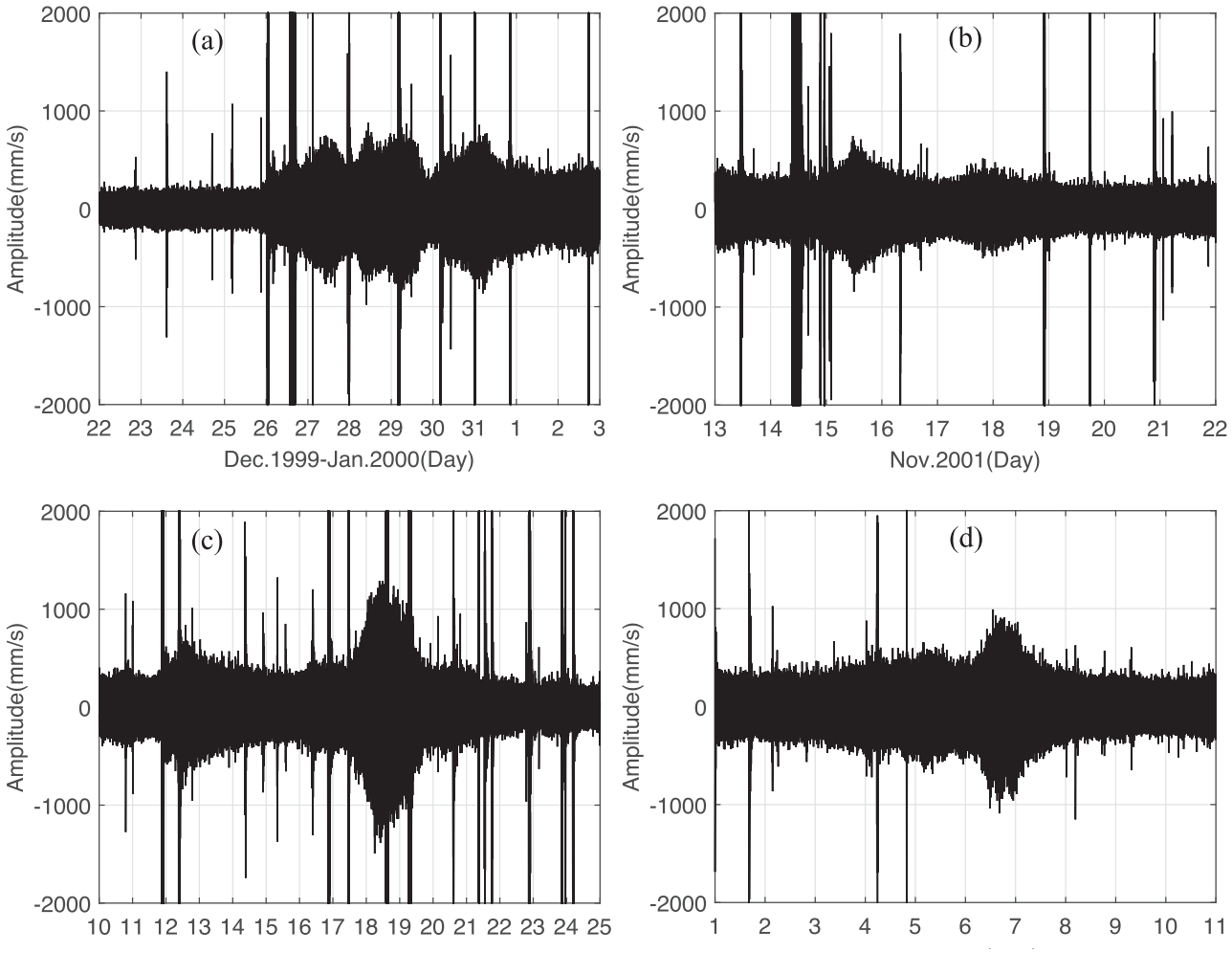

Figure 7. The obvious bulge signals recorded by seismic station WMQ. The emergency time of the peaks of the bulges respectively corresponds to the active times of seven notable European windstorms. (a) Lothar and Martin in 1999 December 26–29 (Brüdl & Rickli 2002). (b) Janika in 2001 December 13–16 (Pellikka & Järvenpää 2003). (c) Erwin (Gudrun) in 5–12 January (Suursaar *et al.* 2006) and Gero in 2005 January 10–19 (Bancroft 2005). (d) Anne in 1–6 January and Christina in 2014 January 3–10 (Burt 2014). The active times of the windstorms can also be obtained from the list of European windstorms on the web page of Wikipedia https://en.m.wikipedia.org/wiki/List_of_European_windstorms.

sequence of monthly PSD is computed by averaging daily PSD over a month.

In the following sections, detailed time-frequency analyses of the big bulge signals recorded by Eurasia stations are presented in Section 3; locating source region of the bulge signals is performed in Section 4. The influence of North Atlantic windstorms on the seismic noise levels in the Central Eurasia is discussed in Section 5.

3 THE TIME–FREQUENCY ANALYSES OF THE BIG BULGE SIGNALS IN EURASIA

For the Eurasia stations investigated in this study (Fig. 1), bulge signals occurring on 2001 November 11 are very big in Northern Europe but they are weak in Southeast Asia. It is noted that some stations having big bulges are located very far from the epicentre of the 2001 Kunlun earthquake. I compared amplitudes of bulge signals at station WMQ, WUS, ARU, OBN, KIEV, KONO and MOL (Figs 1 and 2). These stations are located between Central Eurasia to the Norwegian coast. Fig. 2 shows that the peaks of bulge signals at those stations occur almost simultaneously on 11 November, and the coastal station MOL has the largest amplitude, while the central-Eurasia station WMQ has the smallest one. In Fig. 2, the results of Fourier analysis reveal that the bulge signals at these stations have similar amplitude spectra, and their main components are concentrated in a narrow frequency band of 0.1–0.125 Hz. The extensive observations suggest that the source region of the big bulges may be located near the Norwegian coast, and the big bulge recorded by many Eurasia station is most likely a secondary microseismic bulge generated by a severe North Atlantic windstorm.

Consulting literature on study of North Atlantic extreme windstorms, I verified that an extremely severe windstorm did occur on 2001 November 11 in the Norwegian Sea. On 10 November a windstorm formed over the Greenland Sea near Iceland and subsequently made its way to the Norwegian Sea where it intensified and became a cyclone on 11 November (Reistad *et al.* 2011). The cyclone, being the largest one ever recorded in Norwegian Sea (Feng *et al.* 2012), was so great that it generated sea waves with the average height over 10 m and the maximum height was up to 25.6 m on 11 November. However, this super cyclone has not been named and thus it has

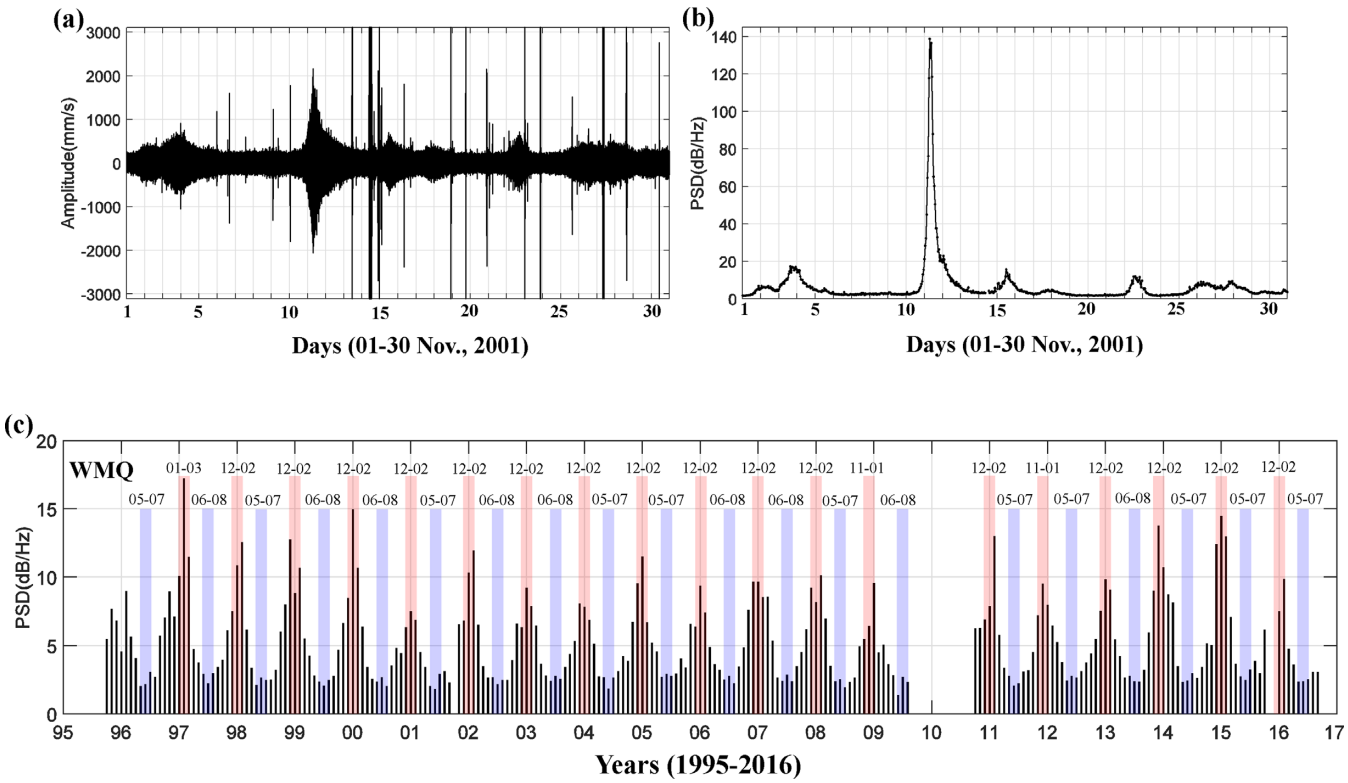

Figure 8. An example showing the calculation of microseism PSD sequences. (a) Vertical data (LHZ) recorded in November, 2001 at station WMQ. (b) Hourly sequence of PSD for the data in the period band of 4–16 s. The result indicates that earthquake signals are clearly removed. (c) Monthly sequence PSD between 1995 and 2016 at WMQ. Color bars in the PSD figure indicate the months in which peaks and troughs of seismic noise levels appear, and the numbers on the top of the bars are month ordinals.

not been well known, presumably due to small hazards it caused. Thus, it was most likely the North Atlantic super cyclone caused strong a microseismic bulge which was widely recorded by seismic stations in Central Eurasia on 11 November before the 2001 Kunlun earthquake.

The microseismic bulge caused by the North Atlantic cyclone is weak signal at continental Asia stations far from the Norwegian coast. For Chinese seismic station KMI (see its location in Fig. 1), the bulge is invisible as local seismic noise is mainly generated by storms of the West Pacific Ocean (Fig. 3a). However, the bulge becomes apparent after filtering data into the narrow frequency band of 0.0938–0.125 Hz by the orthogonal wavelet-packet filter (Fig. 3b).

Fig. 4 shows filtered seismic noise signals in 0.0938–0.125 Hz at ten seismic stations, which located in Eurasia to North America (see map of Fig. 1). The microseismic bulge is also evident at the station SSE close to the Pacific coast of China. However, no bulge is identified at Canadian stations RSSD and LLLB at the same time. It is noted the distance from the Norwegian Sea to SSE, about 9000 km, is much greater than that to RSSD or to LLLB, only about 3500 km. The amplitude of secondary microseism recorded at a seismic station is a function of the amplitude of microseism source, the propagation distance between the source and the station and the structure of the propagation path, as Rayleigh waves are attenuated during their propagation. The observations imply that secondary microseisms generated by the Arctic cyclone near the Norwegian coast are attenuated slowly when they propagate in Eurasia but rapidly during their propagation in North America.

4 LOCATING A SOURCE REGION OF THE BIG BULGE EVENT

I try to define a source region that produced the large bulge signals by polarization analyzing the bulge signals in 0.0938–0.125 Hz (about 8–10 s) at 15 Eurasia stations, which have excellent data quality. The 20-hr bulge data at each station is parsed into 157 segments, 1800 s per segment and overlapping with each other by 75 per cent. The estimation of backazimuth has been performed following the procedure described in Section 2. In each segment, polarization analysis finds out data points that have instantaneous elliptical motions with a ratio of semi-minor axis to semi-major axis greater than 3, and these points are used for calculation back-azimuth. Backazimuths derived from the 157 overlapping segments in the 20-hr data reveal the range of azimuthal variation for a given station during the bulge event.

An example in Fig. 5 shows in detail the procedure of estimating backazimuthals of bulge signals for seismic station KIEV. Fig. 6 shows ranges of azimuthal variations for 15 stations, and the back projection of their backazimuths defines a source region that is located close to the west coast of Norway and the coast of Scotland/Great Britain. Thus, the big bulge signals in 8–10 s occurring on 2001 November 11 are secondary microseisms caused by the interaction of incoming ocean waves and coastal reflections. This result can confirm the conclusion of Sergeant *et al.* (2013) that accurately modelling 7–10 s noise sources in the North Atlantic Ocean must take into account coastal reflections.

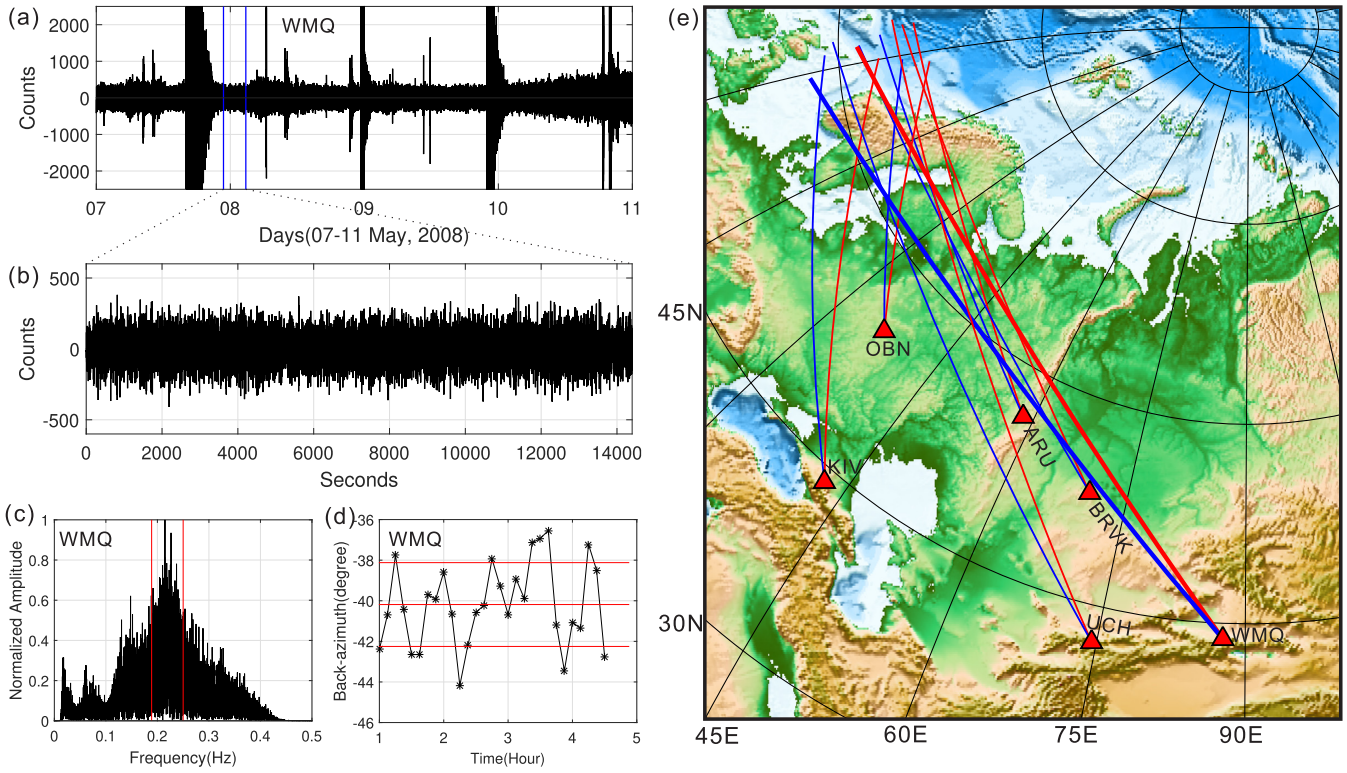

Figure 9. The procedure of locating source region of secondary microseisms in Central Eurasia during a period without microseismic bulge signals. (a) Seismic noise data (LHE) at WMQ during 2008 May 07–11. The period between two blue lines is a 4-hr calm period in which no earthquake and microseismic bulge signals occur. (b) Zooming in on the figure in the calm period. (c) Fourier analysis of the 4-hr calm data, indicating that the main component of the data is in 0.19–0.25 Hz. (d) Backazimuth variation of the most likely source region for WMQ, which is the result of polarization analysis of 29 overlapping segments(1800 s in length for each one) in the 4-hr data. (e) Geographical map showing backazimuth ranges for six stations, indicating that the most possible source region of secondary microseisms for Central Eurasia stations is located near the west coast of Norway.

5 SEASONAL VARIATIONS OF SEISMIC NOISE LEVEL IN CENTRAL EURASIA

Every winter strong extratropical cyclones are generated in the North Atlantic Ocean, and some of them producing devastating socioeconomic impacts in Europe are called European windstorms. These North Atlantic windstorms are given names and their active time and tracks are recorded. Seismic stations in Central Eurasia, such as WMQ, are located very far from the North Atlantic Ocean, but they often record significant secondary microseisms of European windstorms. Fig. 7 shows a number of secondary microseismic bulges recorded at WMQ, their peak time corresponding to the active period of seven notorious European windstorms.

To understand how North Atlantic windstorms affects seismic noise level in Central Eurasia, I have investigated seismic noise levels for station WMQ, BJT, KMI and LSA, distributed from Central Eurasia to East Asia. Figs 8(a) and (b) shows time-series of seismograph and sequences of hourly PSD of seismic noise at WMQ in November 2001, which indicates that earthquake signals are clearly removed and seismic noise level caused by the severe windstorm on 11 November is very high. Sequences of monthly PSD are computed over the years 1996–2016 following the procedure described in Section 2.

Fig. 8(c) shows the sequences of monthly PSD in 20 yr for WMQ located in Central Eurasia. Seismic noise levels at WMQ exhibit obvious seasonal variations, with their peaks usually appearing during December to February in local winter, and their troughs during May to August in local summer. The seasonal dependence of seismic noise spectra for continental stations has been observed by previous studies, with large amplitude during local winter (e.g. Stutzmann *et al.* 2000, 2009; Aster *et al.* 2008). The observation of PSD variations and the polarization analysis of the bulge signals at WMQ imply that seasonal fluctuation of seismic noise levels in Central Eurasia may be mainly caused by variations of North Atlantic windstorms. To confirm this speculation, I try to locate secondary microseismic source region for WMQ in a microseismic calm period (no microseismic bulge events) by using the polarization analysis method similar to that used in Section 4. Polarization analysis is performed for filtered data in the frequency band of 0.19–0.25 Hz, as Fourier analysis shows that the main component of seismic noise in the calm period is in this band (see Figs 9a–c). A variation of backazimuths for WMQ in the calm period is displayed in Fig. 9(d). The ranges of azimuthal variations for six stations are shown on the map in Fig. 9(e), and the back projection of the backazimuths indicates that the source region of secondary microseisms in 0.19–0.25 Hz is most likely located near the Norwegian coast. This result reveals that secondary microseisms in Central Eurasia mainly originate from North Atlantic Ocean, which indicates that the changes in North Atlantic windstorm cause seasonal fluctuations in the level of seismic noise in Central Eurasia.

Fig. 10 shows sequences of monthly PSD in 20 yr for station BJT, KMI and LSA. Station BJT located between central Eurasia and East Asia, and their seismic noise levels also show obvious periodic variations. A little different from the situation at WMQ, seismic noise levels at BJT usually have their peak amplitudes during November to January and sometimes have very large amplitudes

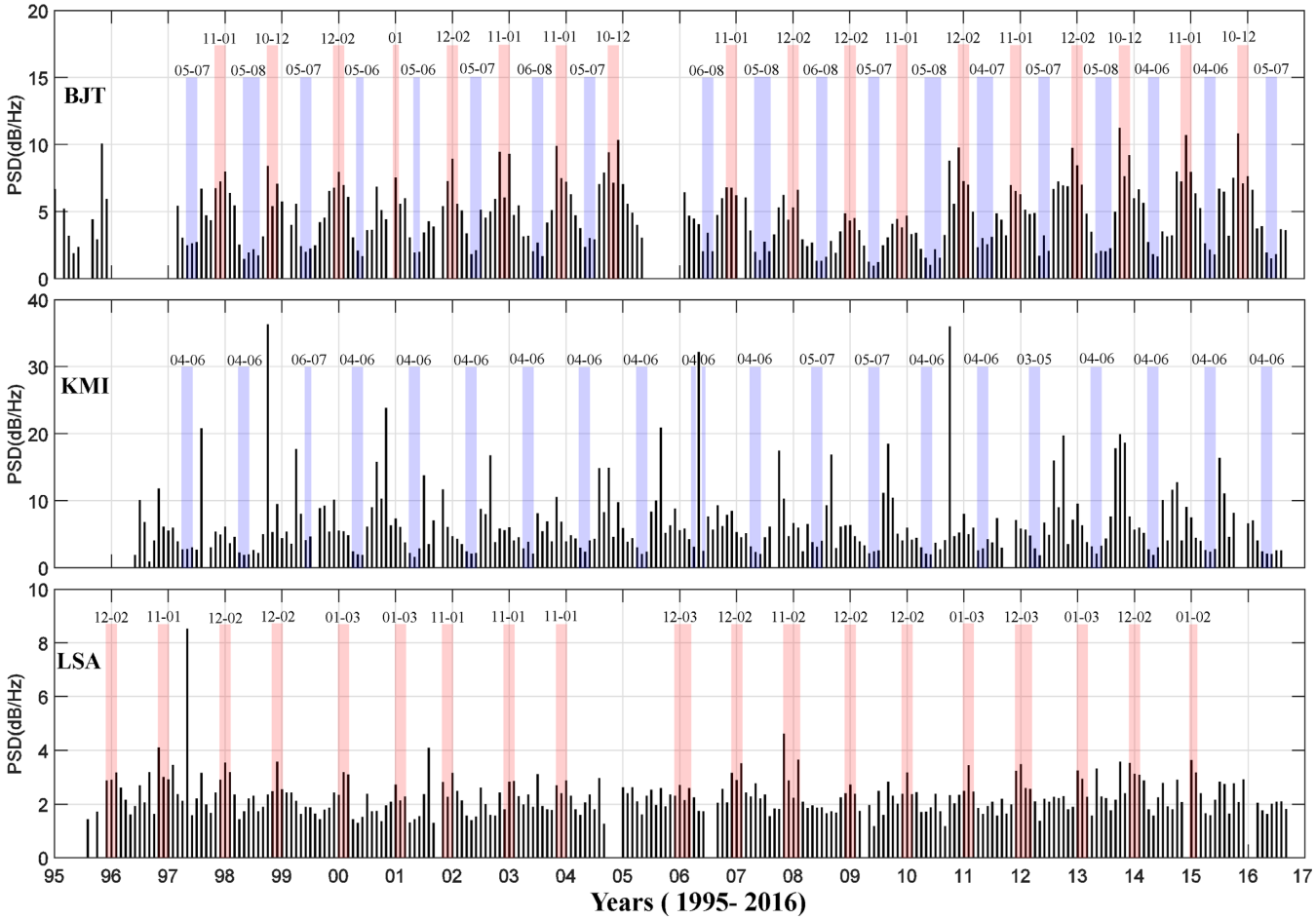

Figure 10. Monthly sequence PSD of vertical data (LHZ) at BJT, KMI and LSA, between January 1995 and August 2016. Color bars in the figure indicate months in which peaks and troughs of seismic noise levels occur. The numbers on the top of the colour bars are month ordinals.

in local autumn. This situation suggests that the seasonal fluctuation of seismic noise levels at BJT may be affected by both the North Atlantic and West Pacific windstorms. For station KMI located in East Asia, seasonal variation of seismic noise levels can only be identified by their troughs usually appear during April to June because of the interference of strong typhoons. The peaks of seismic noise levels at KMI appear in the months when typhoons are very active, showing local sensitivity of seismic noise to West Pacific typhoons near the China Pacific Coast during July to October.

Station LSA is located in Tibet near the North Indian Ocean. Seasonal fluctuation of seismic noise levels at LSA is muted but can be identified by large amplitudes often appearing during December to February in local winter. Large amplitudes of seismic noise levels sometimes occur in other months, which may be caused by strong Indian Ocean cyclones or West Pacific typhoons. For example, the largest amplitude in May 1997 is caused by the North Indian Ocean cyclone during 14–20 May, an extremely severe cyclonic storm named 01B.

On the average, LSA has the lowest average of seismic noise levels in Eurasia, presumably due to strong attenuation of secondary microseisms in the Tibetan Plateau. Rayleigh waves across the Tibetan Plateau are strongly attenuated (Bird & Toksöz 1977), and secondary microseisms are predominantly fundamental mode Rayleigh waves (e.g. Tanimoto & Riveira 2005; Tanimoto *et al.* 2006). Then, secondary microseisms propagating to LSA either from the North Indian Ocean or from the West Pacific and the Arctic and North Atlantic Ocean are strongly attenuated by the Tibetan Plateau. Strong attenuation of Rayleigh waves in Tibet may explain why secondary microseism signals caused by North Atlantic windstorms are strong but those by West Pacific typhoons are weak in Central Eurasia, although secondary microseisms originated from the North Atlantic Ocean travel a much longer distance than those from the West Pacific Ocean do. The Tibetan Plateau has an average elevation of 5.0 km over 7×10^5 km^2. Partially melted rocks below Tibet's crust form a single layer that significantly attenuate long period (40–50 s) Rayleigh waves, which is centred at 70 km below the surface (e.g. Bird & Toksöz 1977). On their way from the coast of the West Pacific Ocean to Central Eurasia, Rayleigh waves of secondary microseisms have to cross the Tibetan Plateau and thus are strongly attenuated.

Figs 11 and 12 show examples that the Tibetan Plateau significantly attenuates strong secondary microseisms caused by severe West Pacific typhoons Neoguri, Son-tinh and Chanchu. Stations KMI and XAN, located between the Tibetan Plateau and Pacific Ocean, recorded large microseismic bulges caused by the typhoons near China Pacific Coast, but stations LSA and WMQ, located on and behind the Tibetan Plateau, recorded no bugles at the same time. Especially, typhoon Son-tinh on 2012 October 28 near Hainan Island of China generated a very large bulge in the recordings at KMI but not any sign of it at LSA and WMQ. It is noted that the

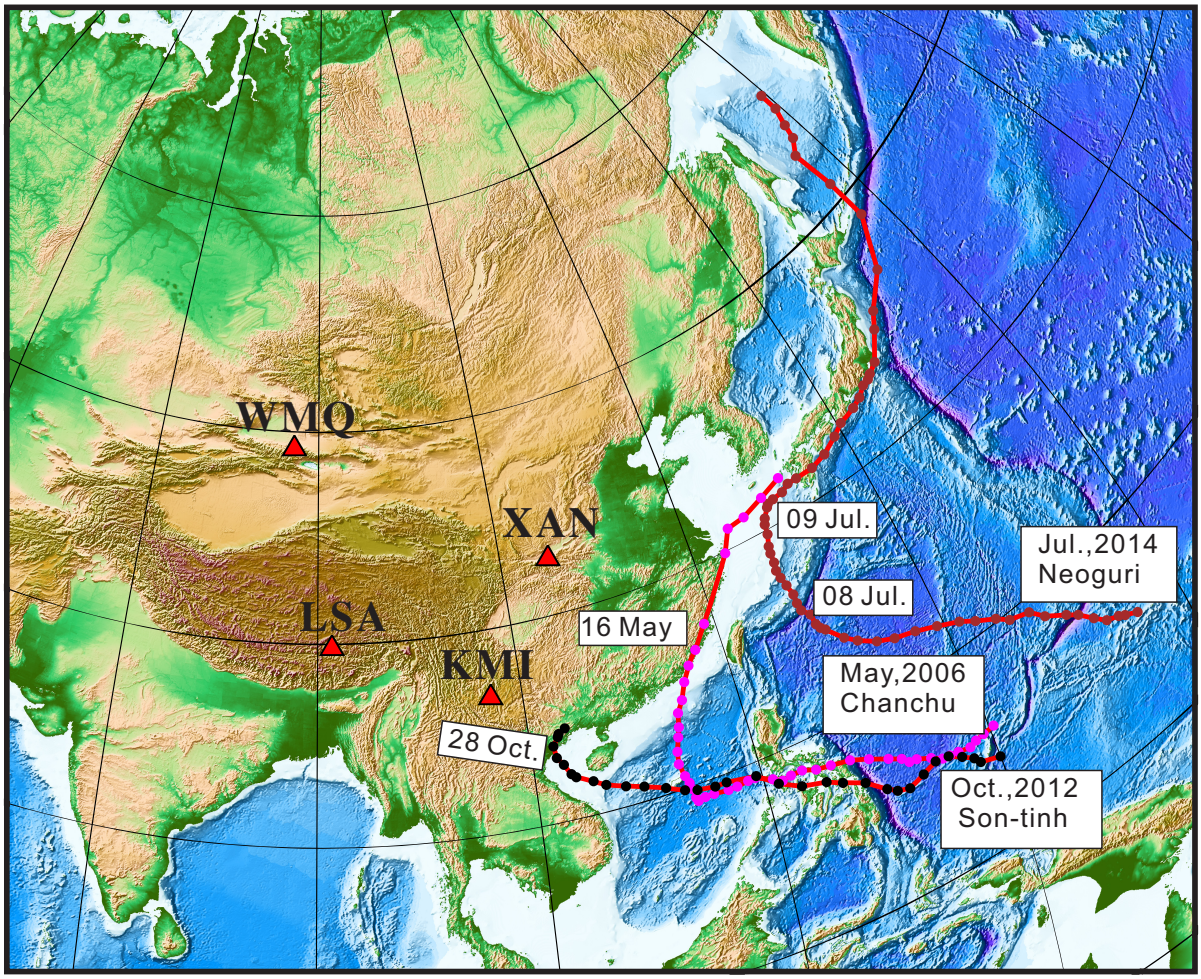

Figure 11. Geographical map showing the tracks of three strong West Pacific typhoons, Neoguri, Son-tinh and Chanchu, close to the Pacific coast of China. Red triangles on the map represent four Chinese seismic stations, which are located in front of, above and behind the Tibetan Plateau. Text boxes next to the tracks indicate the names of typhoons and the years and months of their occurrence, as well as the dates of formation of large bulge signals at stations KMI and XAN.

distance between KMI and LSA is only about 1250 km. No microseismic bulge signals occurring at WMQ further confirms that North Atlantic windstorm plays a leading role in generating seasonal fluctuation in the level of seismic noise in Central Eurasia.

The secondary microseisms caused by typhoons are mainly short-period Rayleigh waves [about 0.13–0.27 Hz (3.7–7.7 s), see Fig. 12]. Strong attenuation of the secondary microseisms of 3.7–7.7 s in Tibet suggests the existence of an attenuating layer at depth much less than 70 km below the surface of Tibet, which confirms the conclusion that Tibet also has a melted or partially melted granitic magma at 10–40 km depth [The comprehensive scientific expedition to the Qinghai-Xizang (Tibetan) Plateau, Chinese academy of sciences, 1980; Wu & Zeng 1996].

6 CONCLUSIONS

Analysis of recordings at stations widely distributed in Eurasia has enabled us to show that big bulge signals recorded in Central Eurasia before the 2001 November 14 M_w7.8 KunLun earthquake are strong secondary microseisms caused by an extremely severe North Atlantic cyclone. Wavelet and polarization analysis of the secondary microseisms in the time-frequency domain enables us to define a sources region of the big bulge, which is located along the west coast of Norway and the coast of Scotland/Great Britain. This analysis method allows us to track secondary microseism source variations.

Wavelet analysis of secondary microseismic signals in a narrow frequency band at stations in Eurasia and North America shows that secondary microseisms caused by the severe cyclonic storm in the Norwegian Sea can travel much further in Eurasia than in North America, even reach China Pacific Coast, indicating that Rayleigh waves in the period band of 8–10 s are attenuated slowly during their propagation in Eurasia but sharply in North America. North Atlantic windstorms have much more strong influence on seismic noise levels in Central Eurasia than West Pacific typhoons do, due to strong attenuation of West Pacific microseisms in the Tibetan plateau, and thus they play leading roles in generating seasonal fluctuation of seismic noise levels in Central Eurasia. Analysis of the attenuation of North America secondary microseisms originated from Arctic and North Atlantic windstorms may help us to find a region in North America near Arctic, of which has an attenuating structure for Rayleigh waves in 4–10. Analysis of variations of secondary microseismic signals in Central Eurasia over long periods of time may be used to study a long-term local climate change caused by Arctic and North Atlantic windstorms.

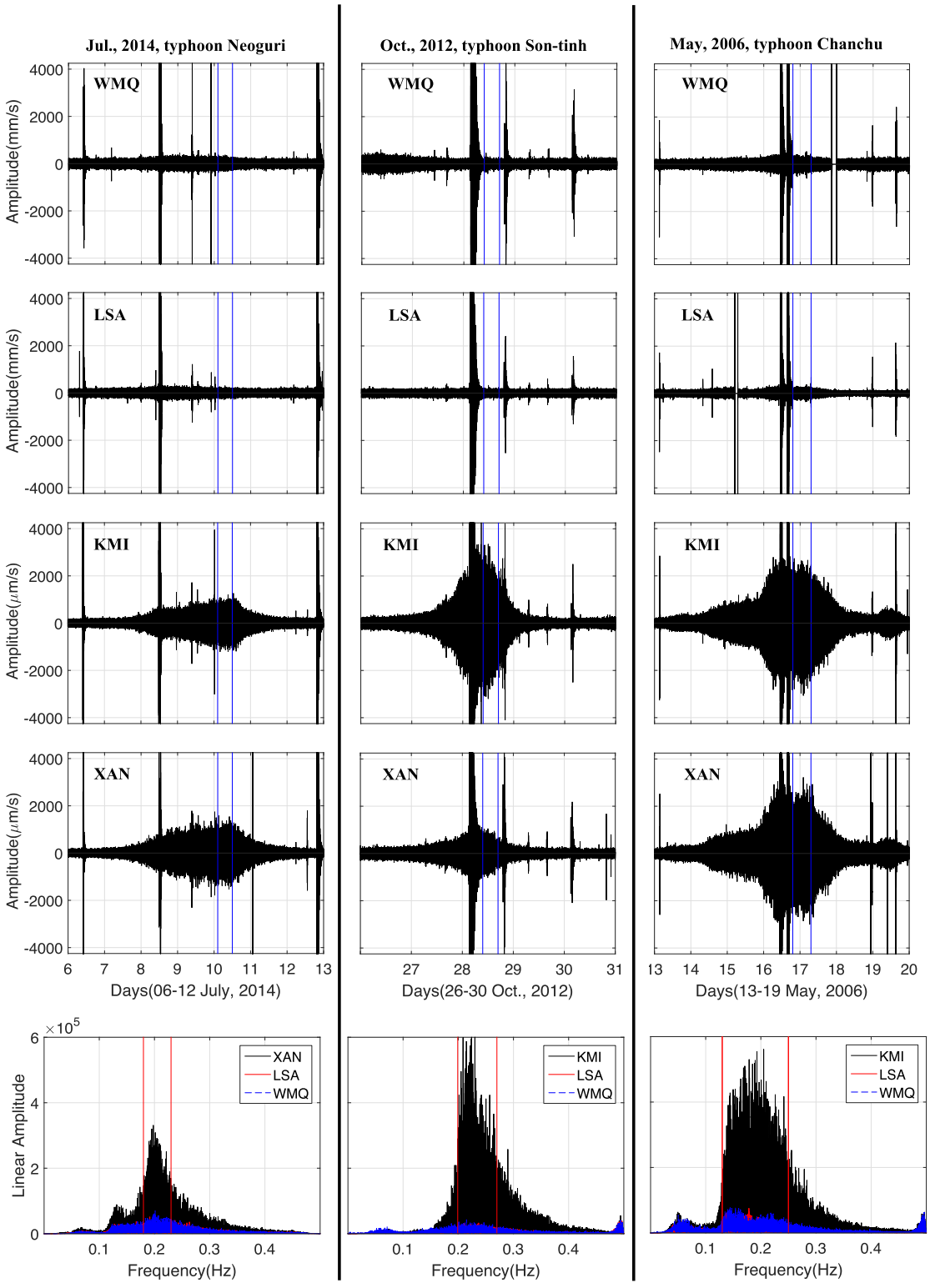

Figure 12. Examples showing that the Tibetan Plateau significantly attenuates the secondary microseisms caused by the three typhoons shown in Fig. 11. Typhoons Neoguri, Son-tinh and Chanchu cause significant bulge signals at KMI and XAN located in front of the Tibetan Plateau, but cause no obvious bulge signals at LSA and WMQ located above and behind the Tibetan Plateau. A Comparison of LSA, WMQ and KMI (or XAN) amplitude spectra shows that the Tibetan Plateau significantly attenuated the strong secondary microseisms caused by the three typhoons. The bulge data used to calculate the spectrum of each station is the time-series between the blue lines. The main components of the bulge signals caused by three typhoons are in the frequency bands of 0.18–0.23, 0.20–0.27 and 0.13–0.25 Hz, which are indicated by red lines in the spectrum diagrams. The track data of the 3 typhoons are provided by the Regional Specialized Meteorological centre (RSMC) Tokyo-Typhoon Center, which can be downloaded from its archive Best Track Data at http://www.jma.go.jp/jma/jma-eng/jma-center/rsmc-hp-pub-eg/trackarchives.This URL is Modified as: Japan Meteorological Agency website (http://www.jma.go.jp/jma/jma-eng/jma-center/rsmc-hp-pub-eg/besttrack.html)

ACKNOWLEDGEMENTS

This work has been carried out thanks to the financial support of the National Science Foundation of China (NSFC) projects (Grant Nos. 41321063, 41174022, 41021003 and 41674100). The author appreciates IRIS/MDC for making seismic data available.

REFERENCES

Aster, R., McNamara, D. & Bromirski, P., 2008. Multidecadal climate-induced variability in microseisms, *Seismol. Res. Lett.,* **79**(2), 194–202.

Bancroft, G.P., 2005. Marine weather review-North Atlantic Area January through April 2005, *Mariners Weather Log,* **49,** 2, August 2005.

Bird, P. & Toksöz, M.N., 1977. Strong attenuation of Rayleigh waves in Tibet, *Nature,* **266**(5598), 161–163.

Behr, Y., Townend, J., Bowen, M., Carter, L., Gorman, R., Brooks, L. & Bannister, S., 2013. Source directionality of ambient seismic noise inferred from three-component beamforming, *J. geophys. Res.,* **118,** 240–248.

Brooks, L.A., Townend, J., Gerstoft, P., Bannister, S. & Carter, L., 2009. Fundamental and higher-mode Rayleigh wave characteristics of ambient seismic noise in New Zealand, *Geophys. Res. Lett.,* **36,** L23303, doi:10.1029/ 2009GL040434.

Burt, S., 2014. Britain's lowest barometric pressure since 1886, *Weather,* **69**(3), 79–81.

Brüdl, M. & Rickli, C., 2002. The storm Lothar 1999 in Switzerland- an incident analysis, *Forest Snow Landscape Res.,* **77,** 207–216.

Cessaro, R., 1994. Sources of primary and secondary microseisms, *Bull. seism. Soc. Am.,* **84**(1), 142–148.

Chevrot, S., Sylvander, M., Benahmed, S., Ponsolles, C., LefeÀvre, J. & Paradis, D., 2007. Source locations of secondary microseisms in western Europe: Evidence for both coastal and pelagic sources, *J. geophys. Res.,* **112,** B11301, doi:10.1029/2007JB005059.

Daubechies, I., 1992. Ten lectures on wavelets, in *CBMS-NSF Reg. Conf. Series Appl. Math,* pp. 61, SIAM.

Feng, X., Tsimplis, M. & Yelland, M., 2012. Extreme waves at Polar front of North Atlantic from 2000 to 2009, *Geophys. Res. Abstracts,* **14,** EGU 2012-5719-1.

Friedrich, A., Kruger, F. & Klinge, K., 1998. Ocean-generated microseismic noise located with the Grafenberg array, *J. Seismol.,* **2**(1), 47–64.

Fu, B. & He, W., 2005. Complex geometry and segmentation of the surface rupture associated with the 14 November 2001 great Kunlun earthquake, northern Tibet, China, *Tectonophysics,* 43–63, https://doi.10.1016/j.tecto.2005.07.002

Galiana-Merino, J.J., Parolai, S. & Rosa-Herranz, J., 2011. Seismic wave characterization using complex trace analysis in the stationary wavelet packet domain, *Soil Dyn. Earthq. Eng.,* **31**(11), 1565–1578.

Gerstoft, P. & Tanimoto, T., 2007. A year of microseisms in southern California, *Geophys. Res. Lett.,* **34,** L20304, doi:10.1029/2007GL031091.

Hasselmann, K., 1963. A statistical analysis of the generation of microseisms, *Rev. Geophys.,* **1,** 177–209.

Hewson, T.D. & Neu, U., 2015. Cyclones, windstorms and the IMILAST project, *Tellus A: Dyn. Meteorol. Oceanogr.,* **67**(1), 27128.

Hu, X.G., Liu, L.T., Ducarmec, B., Hsua, H.T. & Sun, H.-P., 2006a. Wavelet filter analysis of local atmospheric pressure effects in the long-period tidal bands, *Phys. Earth planet. Inter.,* **159,** 59–70.

Hu, X.G., Liu, L.T., Ducarmec, B., Hsua, H.T. & Sun, H.-P., 2006b. Wavelet filter analysis of atmospheric pressure effects in the long-period seismic mode band, *Phys. Earth planet. Inter.,* **154,** 70–84.

Hu, X.G., Liu, L.T., Ducarmec, B., Hsua, H.T. & Sun, H.-P., 2007. Estimation of the pole tide gravimetric factor at the chandler period through wavelet filtering, *Geophys. J. Int.,* **169,** 821–829.

Hu, X.G. & Hao, X.G., 2009. Analysis of the influences of typhoon on anomalous tremors before the great Wenchuan and Kunlunshan earthquake, *Chin. J. Geophys. (in Chinese),* **52**(5), 1363–1375.

Koper, K., Seats, K. & Benz, H., 2010. On the composition of earths short-period seismic noise field, *Bull. seism. Soc. Am.,* **100**(2), 606–617.

Li, L. & Cheng, Y., 2002. Preliminary report on the M_S 8.1 Kokoxili (Qinghai, China) earthquake of 14 November 2001, *Episodes,* **25**(2), 95–99

Longuet-Higgins, M., 1950. A theory of the origin of microseisms, *Philos. Trans. R. Soc. Lond., A ,* 1–35.

Martínez-Alvarado, O., Gray, S.L., Catto, J.L. & Clark, P.A., 2012. Sting jets in intense winter North-Atlantic windstorms, *Environ. Res. Lett.,* **7,** 24014.

Mei, S.R., Xue, Y. & Song, Z.P., 2009. Anonymous seismic characteristics before Wenchuan M8.0 and Kunlunsan M8.1 earthquakes and their implications, *Earthquake (in Chinese),* **29,** 1–13.

Pellikka, P. & Järvenpää, E., 2003. Forest stand characteristics and snow and wind induced forest damage in boreal forests, in *Proceedings of the International Conference on Wind Effects on Trees,* pp. 269–276, ed. Ruck, B., Karlsruhe, Germany, 16–18 Sept., 2003.

René, R.M., Fitter, J.L., Forsyth, P.M., Kim, K.Y., Murray, D.J., Walters, J.K. & Westerman, J.D., 1986. Multicomponent seismic studies using complex trace analysis, *Geophysics,* **51,** 1235–1251.

Reistad, M., Breivik, Ø., Haakenstad, H., Aarnes, O.J., Furevik, B.R. & Bidlot, J.-R., 2011. A high-resolution hindcast of wind and waves for the North Sea, the Norwgian Sea and the Barents Sea, *J. geophys. Res.,* **116,** C05019. doi.10.1029/2010JC006402.

Schimmel, M. & Gallart, J., 2003. The use of instantaneous polarization attributes for seismic signal detection and image enhancement, *Geophys. J. Int.,* **155,** 653–668.

Schimmel, M. & Gallart, J., 2004. Degree of polarization filter for frequency-dependent signal enhancement through noise suppression, *Bull. seism. Soc. Am.,* **94,** 1016–1035.

Schimmel, M., Stutzmann, E. & Gallart, J., 2011a. Using instantaneous phase coherence for signal extraction from ambient noise data at a local to a global scale, *Geophys. J. Int.,* **184,** 494–506.

Schimmel, M., Stutzmann, E., Ardhuin, F. & Gallart, J., 2011b. Polarized Earth's ambient microseismic noise, *Geochem. Geophys. Geosyst.,* **12,** Q07014, doi:10.1029/2011GC003661.

Sergeant, A., Stutzmann, E., Maggi, A., Schimmel, M., Ardhuin, F. & Obrebski, M., 2013. Frequency-dependent noise sources in the North Atlantic Ocean, *Geochem. Geophys. Geosyst.,* **14,** doi:10.1002/2013GC004905.

Stutzmann, E., Roult, G. & Astiz, L., 2000. Geoscope station noise level, *Bull. seism. Soc. Am.,* **90,** 690–701.

Stutzmann, E., Schimmel, M., Patau, G. & Maggi, A., 2009. Global climate imprint on seismic noise, *Geochem. Geophys. Geosyst.,* **10,** Q11004, doi.10.1029/2009GC002619.

Suursaar, Ü., Kullas, T., Otsmann, M., Saaremäe, I., Kuik, J. & Merilain, M., 2006. Cyclone Gudrun in January 2005 and modelling its hydrodynamic consequences in the Estonian coastal waters, *Boreal Environ. Res.,* **11**(2), 143–159.

Tanimoto, T. & Riveira, L., 2005. Prograde Rayleigh particle motion, *Geophys. J. Int.,* **162,** 399–405.

Tanimoto, T., Ishimari, S. & Alvizuri, C., 2006. Seasonality inparticle motion of microseisms, *Geophys. J. Int.,* **166,** 253–266.

The comprehensive scientific expedition to the Qinghai-Xizang Plateau, Chinese Academy of sciences, 1980. *Geothermals beneath Xizang (Tibetan) Plateau,* pp. 107–118, Science Press (in Chinese).

Wang, M.D., Han, Y.J. & Guo, X.Y., 2014. Research on anomaly changes of microtremor before strong earthquake, *J. Seismol. Res. (in Chinese),* **1,** 73–78.

Wickerhauser, M.V., 1994. *Adapted Wavelet Analysis from Theory to Software,* A.K. Peters, Ltd.

Wu, J.P. & Zeng, R.S., 1996. Inversion of Q value structure beneath the Tibetan Plateau, *Acta Seismol. Sin.,* **9**(2), 271–278.

Yang, Y.L., Zhao, G.M. & Gao, G.Y., 2003. The slow earthquake event occurring before the west to Kunlun Mountain Pass earthquake of M_S 8.1, *Recent Dev. World Seismol. (in Chinese),* **9,** 1–4.